Available online at www.sciencedirect.com
ScienceDirect
Biochemical and Biophysical Research Communications 352 (2007) 104–110
BBRC
www.elsevier.com/locate/ybbrc

Translocation and interactions of L-arabinose in OmpF porin: A molecular dynamics study

Kourosh Malek [a,b,*], Ali Maghari [a]

[a] Department of Chemistry, Tehran University, P.O. Box 14155-6455, Tehran, Iran
[b] Schuit Institute of Catalysis, ST/SKA, Eindhoven University of Technology, P.O. Box 513, 5600 MB, Eindhoven, The Netherlands

Received 23 October 2006
Available online 10 November 2006

Abstract

The passage of a natural substrate, L-arabinose (L-ARA) through *Escherichia coli* porin embedded in an artificial bilayer, is studied by equilibrium molecular dynamics simulations. We investigate the early stage of translocation process of L-ARA from intra-cellular to extra-cellular side (Int-to-Ext) across the bilayer. The average trajectory path over all L-ARA molecules along with quantum-mechanical configuration-optimizations at PM3 level predict the existence of at least three trapping zones. The common feature within all these zones is that L-ARA remains perpendicular to the channel axis. It is remarkable how the orientation and translational–rotational motion of L-ARA molecule play a role in its transport through OmpF channel. These simulations are important for better understanding of permeation process in OmpF channel. They also provide an insight into the chiral recognition of translocation process in protein nanochannels from substrate and protein prospects and help interpret experiments on permeation process of small dipolar molecules across biological membranes.

Keywords: Diffusion; OmpF; Arabinose; Molecular dynamics; Chiral translocation

Porins, located in the outer membrane of Gram-negative bacteria, represent a class of passive protein channels that facilitate uptake of ions and nutrients [1,2]. OmpF is a trimeric porin channel that resides in the outer membrane of the *Escherichia coli* bacterium and provides a translocation pathway for dipolar molecules, water, and ions [3]. The three-dimensional structure of OmpF porin has been determined to high resolution by X-ray crystallography [4]. Its well-known and extremely stable molecular structure make it a good choice for experimental and computational studies [5,6]. The OmpF structure consists of about 5 nm long tortuous channels with a pore width ranging from 0.5 nm in the most constricted region to about 1.8 nm at the intra- and extra-cellular inlets, Fig. 1a. The narrow constricted region of each hourglass-shaped channel is highly charged due to the presence of L3 loop, formed of three positively charged (R42, R82, R132) and two negatively charged (R113, R117) amino acids [7]. The arrangement of these charges gives rise to a very strong electric field parallel to the plane of the membrane, which is believed to govern the behavior of open channels [5,8]. The permeation properties of OmpF have been the subject of many computational and experimental studies [5,6]. Full atomic molecular dynamics (MD) simulations have been used to investigate transport of ions and water through porin channels [9,10]. Although much progress has been made to better understand the ion-conduction through OmpF channels, less attention has been devoted to the transport of small molecules. Robertson and Tieleman performed non-equilibrium MD simulations to study the transport and interactions of small dipolar molecules such as methyl-glucose and ampicillin through OmpF [11]. In order to overcome the long-time simulation needed for the complete passage of those molecules, the translocation was

* Corresponding author.
E-mail address: K.Malek@tue.nl (K. Malek).

0006-291X/$ - see front matter © 2006 Elsevier Inc. All rights reserved.
doi:10.1016/j.bbrc.2006.10.183

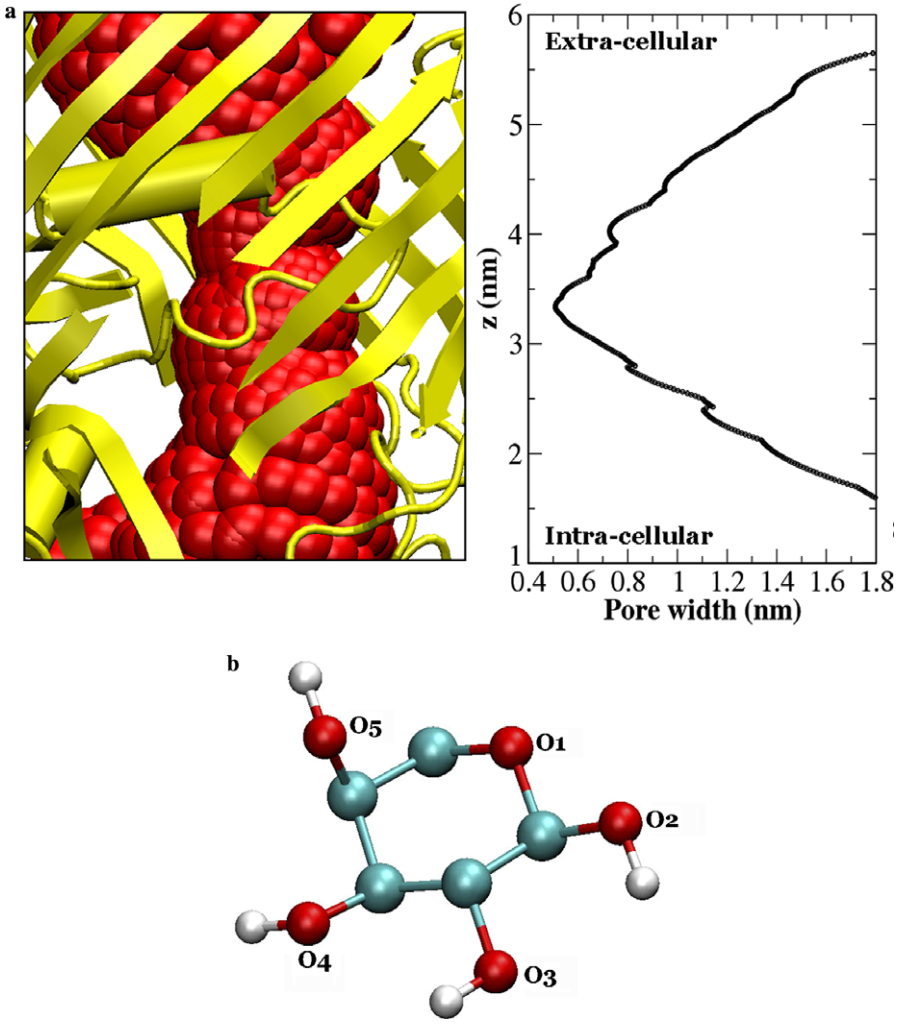

Fig. 1. (a) Visualized pore structure and pore radius profile. The red is the interior profile of the pore while the yellow is the Cartoon representation of OmpF channel (calculated from the starting structure, using HOLE [24]. Some atoms were removed for clarity. Different pore regions are evident; intracellular side, constricted (eyelet) region and extracellular side. (b) L-Arabinose molecule in an alL-atom representation with oxygen atom labels. CH_n groups are represented by united atoms. (For interpretation of the references to color in this figure legend, the reader is referred to the web version of this article.)

performed by artificial pulling of the molecules along the OmpF channels. Those simulations provide valuable information of the orientational effects and possible binding of the molecules in the constriction zone. Diffusion properties, however, could not be well described due to artificial motions of the dipolar molecules. An accelerated, "history dependent" MD methodology was recently introduced and applied to investigate antibiotics translocation through OmpF channel [12]. The main result from all of these simulations is that the passage of dipolar molecules depends on both the internal motion and interactions with the charged residues in L3 loop. The shape of the diffusing molecule, i.e. its flexibility and the presence of a functional group on one side, has also strong influences on its orientation and motion inside OmpF channels [11,12].

The present work seeks to further investigate translocation events of a chiral, dipolar molecule through OmpF porin. We apply MD simulations to study the passage of a natural substrate, L-arabinose (L-ARA) through the OmpF channel, Fig. 1b. L-Arabinose has been extensively used as a substrate to probe diffusion properties of porin channels [13,14]. Despite many experimental studies, its microscopic mechanism of translocation is not well understood. Particularly, we study the blockage effects when such a chiral, cyclic sugar performs an intra- to extra-cellular translocation (Ext-to-Int process) and traps near the constriction zone. According to our knowledge, no diffusion of such sugar has yet been investigated from atomistic point. Moreover, chiral recognition of this translocation process is worth of more fundamental studies. Key questions relate to the dynamics of the permeation and, in particular, the interactions of L-arabinose with residues inside the OmpF channel.

Methodology

The simulation system consists of one trimer of OmpF embedded in a slab of pseudoatoms that mimics a bilayer, Fig. 2. The pseudoatoms are

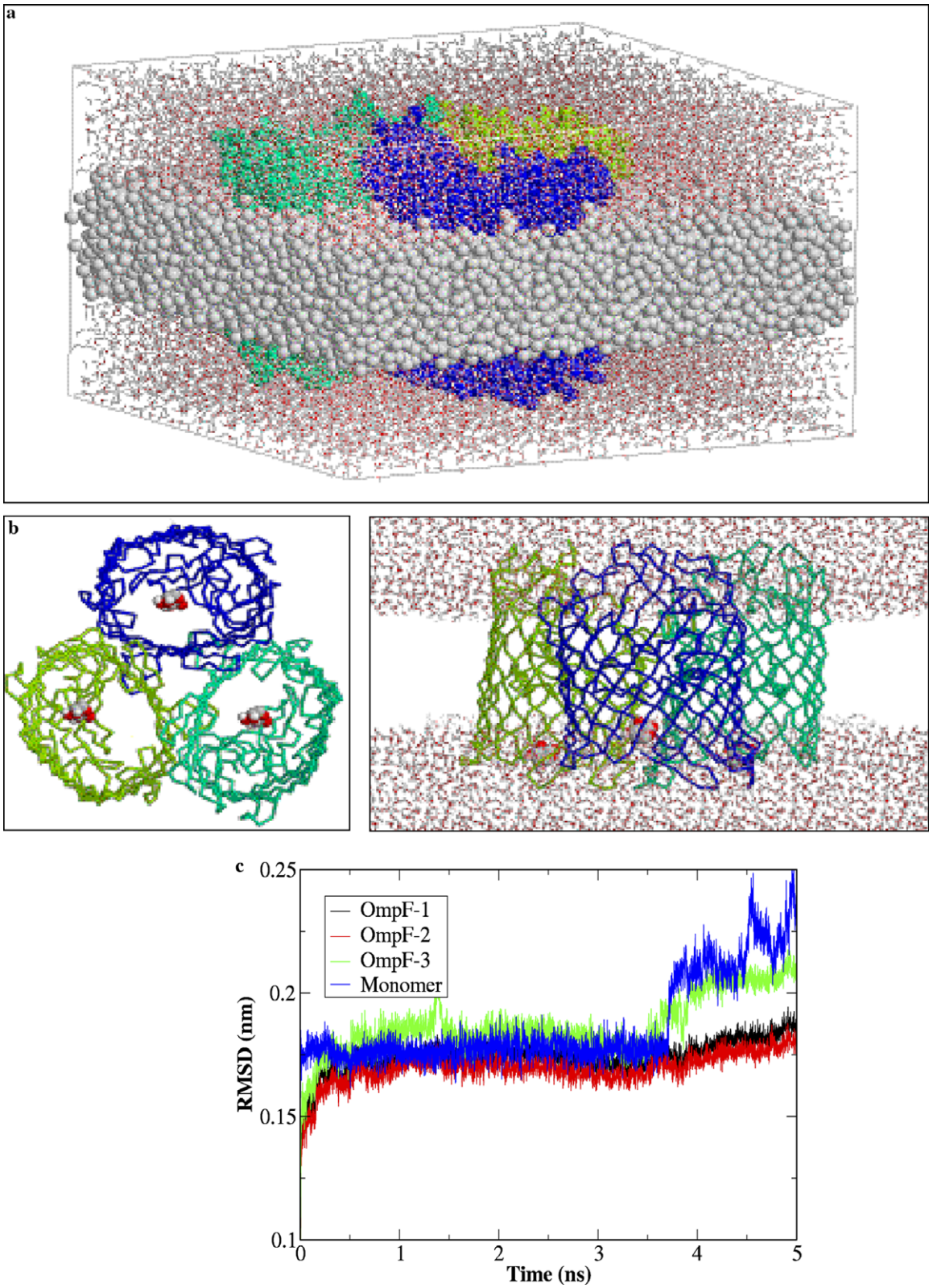

Fig. 2. (a) Snapshot of the OmpF/bilayer simulation system from the front view. (b) The position of L-ARA molecules at the narrowest part of the pore. (c) The C-α root mean square deviation (RMSD) of the individual monomers in a trimer and an isolated monomer, fitted to the initial structure.

uncharged methane molecules and fused around the external surfaces of OmpF trimer during the 1 ns equilibration time. An artificial bilayer permits easy set-up and fast simulations [15]. We did not choose to simulate the transport properties of just one monomer. Although the previous experiments and simulations showed that the three monomers are exactly identical [16], the atomic fluctuation of each individual monomer is unlikely to occur independently. Moreover, at the channel entrance the monomer and trimer are different. L-ARA molecules are placed by hand

near the constriction zone and in the intracellular side (Int) of each OmpF monomer. The system was initially equilibrated for $\tau = 200$ ps using harmonic position restrains (1000 kJ mol^{-1} nm^{-2}). The simple point charge (SPC) model was used to model water [17]. We used GROMOS96 force field [18]. In this force field, interactions between atoms are divided into non-bonded interactions, between any pair of atoms that are within a given cutoff radius, and bonded interactions between atoms connected by chemical bonds. In case of non-bonded interactions (electrostatic and van der Waals), a partial charge and parameters for repulsion and attraction are assigned to each atom. The bonded interaction consists of bond, angle, and dihedral terms. Here, bonds and angles are model led as harmonic oscillators and the dihedral term is represented by a cosine expansion. The most important assumption is that only pair interactions are taken into account (non-bonded interactions between three or more atoms are neglected). To remove the artifacts associated with truncation of electrostatic forces, electrostatic interactions in our simulations were calculated using the Particle-Mesh Ewald (PME) method with a grid spacing of 0.12 nm and fourth order interpolation. MD simulations were performed in a canonical (NVT) ensemble. The temperature was controlled by the Berendsen algorithm, which mimics a weak coupling to an external heat bath at a given temperature T_0. In our simulations, the weak coupling algorithm was applied separately for protein, L-ARA, and solvent plus ions with a time constant $\tau_T = 0.1$ ps and a temperature $T_0 = 300$ K. During the simulation, the potential energy and the total energy were monitored in order to check if the system is in equilibrium. Moreover, the profile of root mean square deviation from the initial configuration was used in order to determine the equilibrium and stability of the OmpF structure. A cutoff of 1.4 nm was used for van der Waals interactions in our simulations. The integration time step was 2 fs. During the production run, structures were saved every 500 steps (1 ps) and used for analysis. Simulations were done with the GROMACS package [19,20] (http://www.gromacs.org). Visualization was done by using the VMD v1.8.1 [21]. The structure of L-ARA at some points along the MD trajectory was optimized by a quantum-mechanical method by means of PM3 semi-empirical calculations [22] and using GAUSSIAN03 package [23].

Results and discussion

We describe and quantify the motion and orientation of L-ARA molecules inside OmpF channel observed in the simulations. Hydrogen bonds, number of contacts, and minimum distance between L-ARA molecule and the OmpF residues as well as dipole moment of L-ARA are used as coordinates to analyze the translocation process. Besides, quantum-mechanical calculations are performed at the PM3 level in order to optimize the structure of L-ARA at some points along the trajectory of L-ARA molecule inside the OmpF channel.

After the system was relaxed for 200 ps, we placed L-ARA molecules by hand near the constriction zone and in the intracellular side (Int). The resulting structure was energy minimized for another 200 ps. The translocation in our simulation is taking place from intracellular (Int) to extracellular (Ext) side. There is no reference coordinate for the initial configuration of the L-ARA molecules, however, the selected positions provide general feature of a minimum potential well [12]. The configuration was chosen such that it contains the contacts between L-ARA and charged amino acids located at the channel inlet. L-ARA is surrounded by ARG270, GLU48, ASP12, and LYS46. Particularly, O3 interacts with GLU48, ARG270, and LYS46, while O2 interacts with ASP12 and O1 is pointing toward the inlet region. Fig. 2c illustrates the root mean square deviation of C-α for the L3 loop of the individual monomers with respect to the crystal structure. The C-α atoms of each L3 loop of each monomer are fitted separately. The green line in Fig. 2c also shows the RMSD of the L3 loop for an isolated monomer in the bilayer, resulting from an independent simulation. The RMSD for L3 loop slowly increases, from 0.12 to 0.2 nm during 5 nanoseconds (ns). The RMSD profile for the monomers is not identical, as a result of different dynamical behavior of L-ARA. Monomer 3 shows dramatic fluctuations at times 1.5 and 4 ns, while the profile remains identical for the two other monomers. It is also interesting to compare the behavior of an isolated monomer and that of monomers in a trimer. The isolated monomer shows a different profile, which indicates that the translocation of L-ARA in an isolated monomer is not necessarily identical to that in the individual monomers of a trimer. To understand the origin of such differences, we should notice that the dynamics of L-ARA affects the motion of L3 loop inside the OmpF. It was also shown that the pore size of OmpF fluctuates during the MD simulations [9]. The most important source of difference between monomers relates to conformational distortion in α-helical structure of residues 105–112 of the L3 loop. The helix presents in monomers 1 and 2, whereas in monomer 3 part of the helix acquires 1–3 helix conformation [8,9]. Therefore, the conformational fluctuations of α-helical structure of the L3 loop along with the different dynamical motion of L-ARA in three monomers caused non-identical RMSD profiles.

Fig. 3a illustrates the time-dependent displacement of L-ARA molecules along the OmpF channel during 5 ns dynamics. The OmpF channels are located between 1.0 (Int) and 6.0 nm (Ext). A few notable events are observed. L-ARA molecules remain inside the channels during 5 ns dynamics. Fig. 3a shows that L-ARA molecules are trapping inside the channel at some locations, while their positions considerably fluctuate. The electrostatic and dipole–dipole interactions inside the channel are very essential for such dynamical motion. To explain this observation, we calculated the total dipole moment of each L-ARA molecule inside the OmpF channel. Fig. 3b shows the average dipole moment (μ_z) of L-ARA, with respect to the z-position. The maximum magnitude of μ_z for each L-ARA molecule is about 0.5 D. Close to residue ARG270 and LYS16 at the channel inlet ($2 < z < 3$ nm) there is a strong peak for L-ARA-3 in the graph. In this region the O1 of L-ARA-3 preferentially orients itself toward the constriction zone. In the constriction zone between 3 and 4 nm, there is no preferential orientation, so that this L-ARA molecule does not enter further into the channel. It is remarkable how the L-ARA molecule changes its orientations to escape from the potential wells inside the channel. L-ARA-1, for instance, reorients itself in constriction zone, whereas L-ARA-2 does not show any preferential orientation in Int side. Notice that each of these molecules follow a different trajectory path inside the channel, so that they interact with

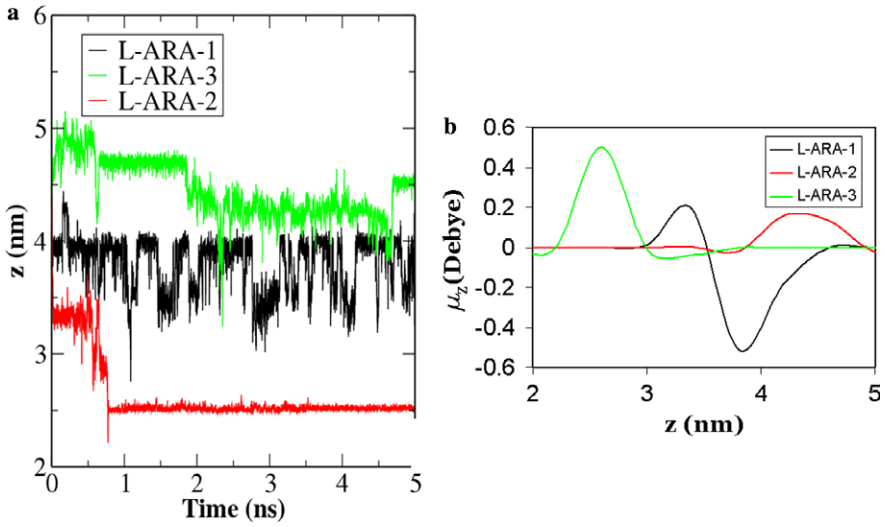

Fig. 3. (a) Positions along the pore z-axis vs. time for all three L-ARA molecules. (b) The z component of the average dipole moment of the chiral L-ARA molecules in respect to z-axis. Zero moment corresponds to no preferential orientation.

different residues while they are trapping into different amino acid cages. In order to capture the energetics of those trapping zones inside the channel, we qualify the phenomena by quantum-mechanical based optimizations. Calculations on the level of semi-empirical PM3 was performed on the last MD frame immediately before escaping from the trapping region. Each calculation is followed by a HF/6-31G* optimization. Fig. 4a shows the final optimized geometries of L-ARA molecules trapped at each potential well. Fig. 4 shows that the first necessary step for L-ARA molecule to escape from each potential well is to reorient itself so that O1 lies toward the Ext-side. Our calculations based on the average trajectory path over all three L-ARA molecules predict the existence of at least three trapping zones. At zone I, L-ARA interacts mostly with LYS167, ASP126, ARG42, GLU62, and ARG82. Optimization in the presence of ASP126, ARG42, and ARG82 shows that O2 and O3 interact strongly with the NH_3 of ARG82, while the other hydroxyl oxygens orient toward ASP126. At zone II, L-ARA traps inside a cage containing ARG270, LYS305, and ASP266. At this region O2 remains close to ARG270 and other hydroxyl groups lie in the surface parallel to the loop L3. Finally at zone III, L-ARA is surrounded by ASP113, ASP312, GLU296, and ARG270. The common feature within all these regions is that L-ARA remains perpendicular to the channel axis. Moreover, it orients itself so that the O1 stays toward Ext-side. Notice that in all the configurations in Fig. 4a the hydroxyl groups are mostly interacts with the NH_3 or COOH terminus of the charged ARG, ASP, GLU, and LYS residues.

More dynamical features of the translocation process are shown in Fig. 4b. Here the degree of interaction between L-ARA and the residues is determined based on number of hydrogen bonds, number of contacts and minimum distance with the first 70 residues located in the first half of the channel at Int-side. There are considerably high number of hydrogen-binding interaction between residues and L-ARA. In the channel inlet, L-ARA molecule forms hydrogen bonds with water and with the amino acids. There are comparably more hydrogen bonds between residues LYS16 (residue number 3) and LYS46(5), which is likely due to the particular orientation of L-ARA in the vicinity of these residues close to the trapping zone I. At this location, O2, O4, and O5 lie toward NH_3 terminus of LYS46 and LYS16, so that a strong hydrogen-binding is evidence. Optimized geometries at this region predicts a minimum distance of 0.18 nm, corresponding to hydrogen bonds. Inside the pore at the constriction zone, the total number of hydrogen bindings increases, however, none of the residues establishes hydrogen bonds as Strong as those in the pore inlet. Similar features are observed from the number of contacts and minimum distance between L-ARA and residues on the channel wall. In the pore inlet, L-ARA molecule shows relatively high number of contacts with LYS16, ARG42, and LYS46 residues, whereas in the constricted zone different paths are followed. It is also interesting to look at the optimized geometries at this zone. At regions II and III, L-ARA remains close to the charged amino acids. However, it is stabilized in such a way that the hydrogen-binding between L-ARA and residues at the constricted zone is less than that at the OmpF inlet. The number of contacts, yet remains high at this region as the trajectory of L-ARA molecule at this region shows. The minimum distances fluctuate between 0.5 and 3.5, corresponding to the dynamical motion of the L-ARA molecule inside the OmpF channel. At region II there is comparably less interactions with residues, due to its specific equilibrium orientation in respect to residues ARG270, LYS305, and ASP266. Although our simulations only deal with one of the enantiomers of arabinose molecule, they can provide some of the features related to the chiral translocation in OmpF. Theoretical models of biological chiral

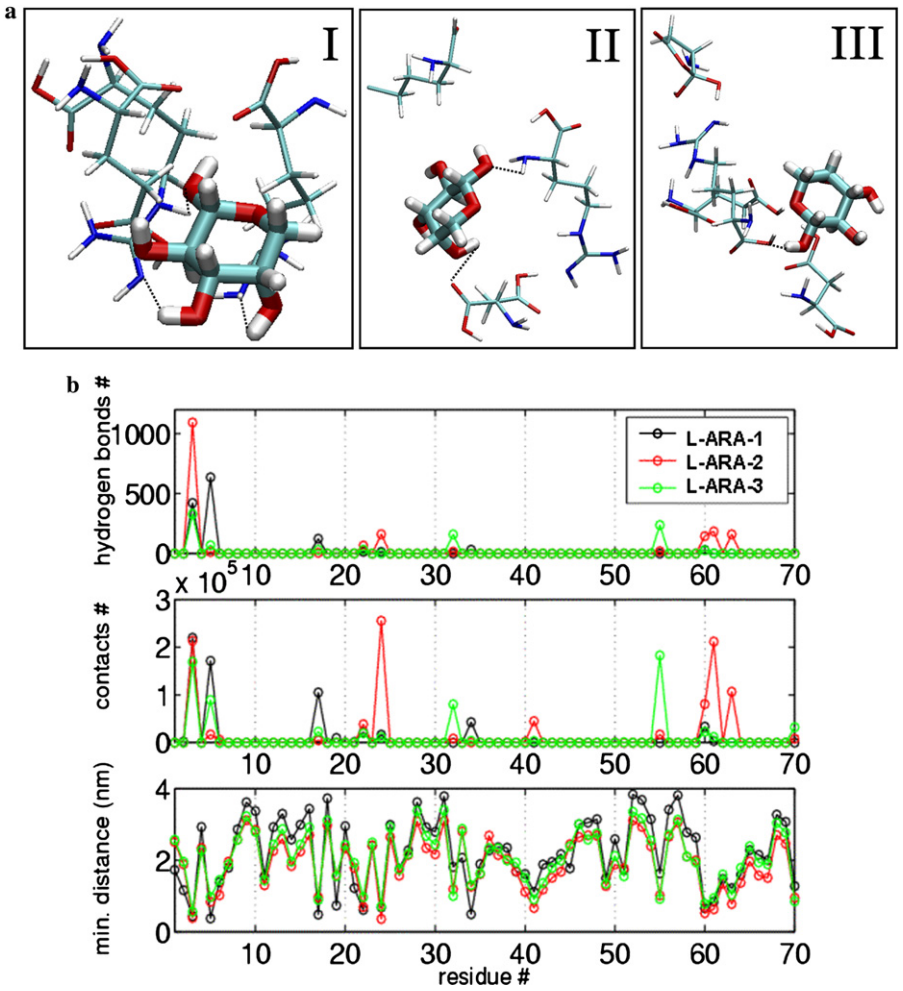

Fig. 4. (a) All-atom representation of the PM3 optimized conformations sampled during the process Int-to-Ext. Contacts: (I) O2-ARG82, O3-ARG82, O5-ASP216; (II) O3-ARG270. (b) Analysis of interaction parameters between L-ARA molecules and first 70 residues in intracellular side in terms of number of hydrogen bonds, number of contacts, and minimum distance: L-ARA-1 (black); L-ARA-2 (red); and L-ARA-3 (green). (For interpretation of the references to color in this figure legend, the reader is referred to the web version of this article.)

recognition such as the three-point attachment (TPA) can be used to explain the differential recognition of a pair of arabinose enantiomers with the single trapping zone (chiral center) inside OmpF channel [25]. However, the prohibitive timescale for any equilibrium MD simulation does not allow to investigate a complete translocation process [16]. It seems likely that combined accelerated MD simulations and a novel stereo-center-recognition model for protein chiral recognition can describe the chiral translocation phenomena more accurately. Nevertheless, the early passage studies, similar to what we presented here, can rationalize general features of such a selective translocation. The main hindrance for the whole translocation process is the strong dipole–dipole and electrostatic interactions at constriction zone, acting as a filter. More features of such interactions can be better studied in course of free energy calculations.

Conclusion

We presented molecular dynamics simulations for translocation of a chiral-dipolar molecule (L-arabinose; L-ARA) through OmpF channel. The simulations reflect general features of the channel's chiral selectivity for L-ARA enantiomer. The analysis of trajectories shows that the L-ARA molecule traps into a few potential wells during its dynamical motions through OmpF channel. Quantum-mechanical optimizations at PM3 level on those trapping zones show that escaping from a potential well is established when the L-ARA molecule reorients toward the extra-cellular side. Our calculations based on the average trajectory path over all three L-ARA molecules predict the existence of at least three trapping zones. At zone I, L-ARA interacts mostly with LYS 167, ASP126, ARG42, GLU62, and ARG82. Zone II consists of ARG270, LYS305, and ASP266. At this region O2 closely interacts with ARG270 and other hydroxyl groups lie parallel to the constriction zone. Finally at zone III, L-ARA is surrounded by ASP113, ASP312, GLU296, and ARG270. Simulations show that during the permeation process, L-ARA aligns into potential wells in the eyelet region. This is mainly caused by electrostatic, hydrogen-binding and dipole–dipole interactions between chiral L-ARA molecule and charged residues of OmpF imposed into

the channel space. As a result, the chiral translocation is considerably slowed down. Our simulation did not show a complete passage during 5 ns dynamics. The early passage study presented here provides the general features of a chiral translocation process in OmpF channel. The results also help to interpret experiments on permeation process of small dipolar molecules across biological membranes.

References

[1] G.E. Schulz, Porins: General to specific, native to engineered passive pores, Curr. Opin. Struct. Biol. 6 (1996) 485–490.

[2] H. Nikaido, Porins and specific diffusion channels in bacterial outer membranes, J. Biol. Chem. 269 (1994) 3905–3908.

[3] S.W. Cowan, T. Schirmer, G. Rummel, M. Steiert, R. Ghosh, R.A. Pauptit, J.N. Jansonius, J.P. Rosenbusch, Crystal-structures explain functional-properties of 2 *Escherichia-coli* porins, Nature 358 (1992) 727–733.

[4] S.W. Cowan, Bacterial porins: Lessons from 3 high-resolution structures, Curr. Opin. Struct. Biol. 3 (1993) 501–507.

[5] D.P. Tieleman, P.C. Biggin, G.R. Smith, M.S. Sansom, Simulation approaches to ion channel structure-function relationships, Q. Rev. Biophys. 34 (2001) 473–561.

[6] W. Im, S. Seefeld, B. Roux, A grand canonical Monte Carlo-Brownian dynamics algorithm for simulating ion channels, Biophys. J. 79 (2000) 788–801.

[7] T. Schirmer, General and specific porins from bacterial outer membranes, J. Struct. Biol. 121 (1998) 101–109.

[8] S. Varma, E. Jakobsson, Ionization states of residues in OmpF and mutants: Effects of dielectric constant and interactions between residues, Biophys. J. 86 (2004) 690–704.

[9] D.P. Tieleman, H.J.C. Berendsen, A molecular dynamics study of the pores formed by *Escherichia coli* OmpF porin in a fully hydrated palmitoyloleoylphosphatidylcholine bilayer, Biophys. J. 74 (1998) 2786–2801.

[10] E.M. Nestorovich, T.K. Rostovtseva, S.M. Bezrukov, Residue ionization and ion transport through OmpF channels, Biophys. J. 85 (2003) 3718–3729.

[11] K.M. Robertson, D.P. Tieleman, Orientation and interactions of dipolar molecules during transport through OmpF porin, FEBS Lett. 528 (2002) 53–57.

[12] M. Ceccarelli, C. Danelon, A. Laio, M. Parrinello, Microscopic mechanism of antibiotics translocation through a porin, Biophys. J. 87 (2004) 58–64.

[13] D.S. Dwyer, Model of the 3-D structure of the GLUT3 glucose transporter and molecular dynamics simulation of glucose transport, Protein: Structure, Function and Genetics 42 (2001) 531–541.

[14] E. Sugawara, H. Nikaido, OmpA protein of Escherichia-coli outer membrane occurs in open and closed channel forms, J. Biol. Chem. 269 (1994) 17981–17987.

[15] D.P. Tieleman, J.L. MacCallum, W.L. Ash, C. Kandt, Z. Xu, L. Monticelli, Membrane protein simulations with a united-atom lipid and all-atom protein model: lipid-protein interactions, side chain transfer free energies and model proteins, J. Phys: Condens. Matter 18 (2006) S1221–S1234.

[16] W. Im, B. Roux, Ions and counterions in a biological channel: A molecular dynamics simulation of OmpF porin from Escherichia coli in an explicit membrane with 1 M KCl aqueous salt solution, J. Mol. Biol. 319 (2002) 1177–1197.

[17] H.J.C. Berendsen, J.P.M. Postma, W.F. van Gunsteren, J. Hermans, Intermolecular Forces, Reidel, Dordrecht, 1981.

[18] W.F. van Gunsteren, J.C. Berendsen, Computer-simulation of molecular dynamics methodology, applications and perspectives in chemistry, Angew. Chem. Int. Edn Engl. 29 (1990) 992–1023.

[19] E. Lindahl, B. Hess, D. van der Spoel, GROMACS 3.0: a package for molecular simulation and trajectory analysis, J. Mol. Mod. 7 (2001) 306–317.

[20] H.J.C. Berendsen, D. van der Spoel, R. van Drunen, GROMACS—A message-passing parallel molecular dynamics implementation, Comp. Phys. Comm. 91 (1995) 43–56.

[21] W. Humphrey, A. Dalke, K. Schulten, Visual molecular dynamics, J. Mol. Graph. 14 (1996) 33.

[22] J.J.P. Stewart, Optimization of parameters for semiempirical methods 1: Method, J. Comp. Chem. 10 (1989) 209–220.

[23] J.R. Cheeseman, J.A. Montgomery Jr., T. Vreven, K.N. Kudin, J.C. Burant, J.M. Millam, S.S. Iyengar, J. Tomasi, V. Barone, B. Mennucci, M. Cossi, G. Scalmani, N. Rega, G.A. Petersson, H. Nakatsuji, M. Hada, M. Ehara, K. Toyota, R. Fukuda, J. Hasegawa, M. Ishida, T. Nakajima, Y. Honda, O. Kitao, H. Nakai, M. Klene, X. Li, J.E. Knox, H.P. Hratchian, J.B. Cross, V. Bakken, C. Adamo, J. Jaramillo, R. Gomperts, R.E. Strat-mann, O. Yazyev, A.J. Austin, R. Cammi, C. Pomelli, J.W. Ochterski, P.Y. Ayala, K. Morokuma, G.A. Voth, P. Salvador, J.J. Dannenberg, V.G. Zakrzewski, S. Dapprich, A.D. Daniels, M.C. Strain, O. Farkas, D.K. Malick, A.D. Rabuck, K. Raghavachari, J.B. Foresman, J.V. Ortiz, Q. Cui, A.G. Baboul, S. Cliord, J. Cioslowski, B.B. Stefanov, G. Liu, A. Liashenko, P. Piskorz, I. Komaromi, R.L. Martin, D.J. Fox, T. Keith, M.A. Al-Laham, C.Y. Peng, A. Nanayakkara, M. Challacombe, P.M.W. Gill, B. Johnson, W. Chen, M.W. Wong, C. Gonzalez, J.A. Pople, Gaussian 03, ReVision B01, Gaussian, Inc., Wallingford, CT, 2004.

[24] O.S. Smart, J.G. Neduvelil, X. Wang, B.A. Wallace, M.S.P. Sansom, A program for the analysis of the pore dimensions of ion channel structural models, J. Mol. Graph. 14 (1996) 354.

[25] V. Sundaresan, R. Abrol, Biological chiral recognition: The substrate's perspective, Chirality 17 (2005) S30–S39.